

# CodedVO: Coded Visual Odometry

Sachin Shah<sup>\*1</sup>, Naitri Rajyaguru<sup>\*2</sup>, Chahat Deep Singh<sup>2,3</sup>, Christopher Metzler<sup>†1</sup>, Yiannis Aloimonos<sup>†2</sup>

<sup>\*</sup>Equal Contribution, <sup>†</sup>Equal Contribution

University of Maryland, College Park<sup>1,2</sup>, University of Colorado, Boulder<sup>3</sup>

**Abstract**—Autonomous robots often rely on monocular cameras for odometry estimation and navigation. However, the scale ambiguity problem presents a critical barrier to effective monocular visual odometry. In this paper, we present CodedVO, a novel monocular visual odometry method that overcomes the scale ambiguity problem by employing custom optics to physically encode metric depth information into imagery. By incorporating this information into our odometry pipeline, we achieve state-of-the-art performance in monocular visual odometry with a known scale. We evaluate our method in diverse indoor environments and demonstrate its robustness and adaptability. We achieve a 0.08m average trajectory error in odometry evaluation on the ICL-NUIM indoor odometry dataset.

## I. INTRODUCTION

Over 3.8 billion years of genetic evolution, nature has witnessed remarkable transformations, with a significant focus on the development of visual systems. This journey has taken us from the earliest photoreceptors to the intricate and diverse array of eye structures observed in species like frogs [1] and cuttlefish [2]. This evolutionary trajectory has been purposive and parsimonious [3], predominantly influenced by sensory behaviors and environmental interactions. Evolutionary processes have resulted in these animals and their sensory organs becoming more and more *specialized*. By contrast, today in the field of robotics a *general-purpose* philosophy to sensor design is the norm. For instance, a similar set of cameras is deployed for navigation in both home automation robots and self-driving cars.

Visual odometry (VO) is the cornerstone of robot autonomy, empowering mobile robots to know their location with respect to their surroundings [4]. The inherent variability and complexity of real-world settings present significant challenges for conventional monocular visual navigation approaches, often rendering them impractical in estimating their location [5]. To ameliorate this effect, researchers have employed

Manuscript received: February, 02, 2024; Revised May, 01, 2024; Accepted May, 31, 2024.

This paper was recommended for publication by Editor Pascal Vasseur upon evaluation of the Associate Editor and Reviewers' comments.

<sup>1</sup>UMD Intelligent Sensing Laboratory, University of Maryland Institute for Advanced Computer Studies, University of Maryland, College Park, MD 20742, USA. Emails: {shah2022, metzler}@umd.edu.

<sup>2</sup>Perception and Robotics Group, University of Maryland Institute for Advanced Computer Studies, University of Maryland, College Park, MD 20742, USA. Emails: nrajyagu@terpmail.umd.edu, jyaloimo@umd.edu.

<sup>3</sup>Perception, Robotics, AI, Sensing Lab , University of Colorado, Boulder. Email: chahat.singh@colorado.edu.

The support of ONR under grant award N00014-17-1-2622 is gratefully acknowledged. This work was supported in part by the Joint Directed Energy Transition Office and a seed grant from SAAB, Inc. Chahat Deep Singh is supported in part by the Army Research Laboratory under the ArtAMAS cooperative agreement.

Digital Object Identifier (DOI): see top of this page.

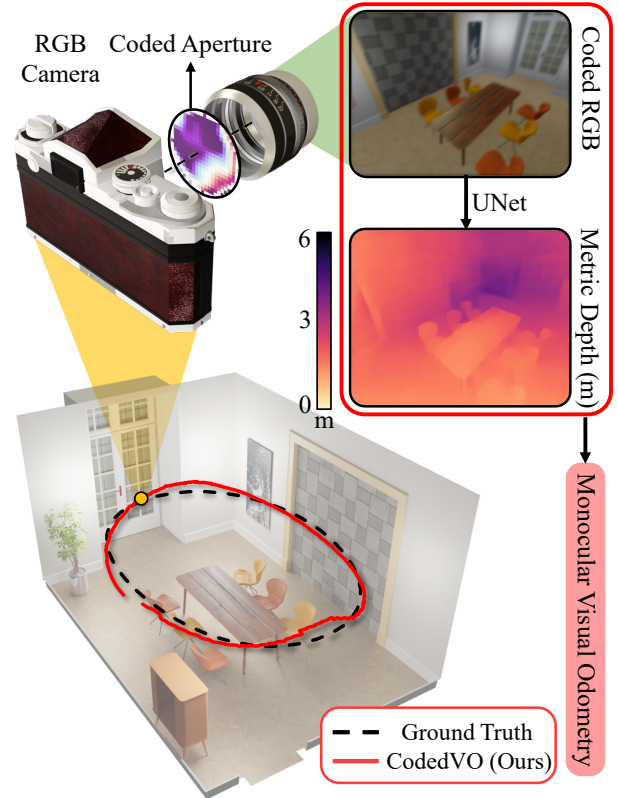


Figure 1: **System Overview.** Our proposed approach leverages coded apertures to predict metric dense depth maps using only an RGB sensor tailored for monocular odometry estimation.

additional sensors that increase the power costs to the system such as an additional camera with a calibrated baseline (stereo setup), active sensors such as infrared depth sensors and/or inertial measurement units (IMU). Since these systems provide the metric unit (or scale) of the scene, they have widely been used in odometry estimation and navigation tasks. In efforts to remove the need for additional sensors in VO, researchers have utilized depth information obtained through monocular depth estimation methods. These techniques produce normalized dense depth maps from monocular RGB images, with Sun et al. (2022) [6] showcasing notable success in odometry benchmarks. However, the absence of scale in these depth assessments poses a challenge, reducing their effectiveness in real-world applications due to the unknown scale factor.

Drawing inspiration from the evolution of eyes and pupils, researchers have employed coded apertures to capture depth information with passive monocular camera systems. These coded aperture systems operate by encoding depth information into defocus blur. While widely employed in scientific imaging [7], to date such methods have been underutilized in

the field of robot autonomy. This paper introduces **CodedVO**, a novel visual odometry method that leverages the metric depth maps from the geometric constraints provided by a coded camera system and achieves state-of-the-art monocular odometry performance.

#### A. Key contributions

- In this paper, we introduce **CodedVO**, a novel method for estimating monocular visual odometry that leverages the RGB and estimates of metric depth obtained through a phase mask on a standard 1-inch camera sensor and demonstrate its generalizability in novel scenes.
- We propose a novel depth-weighted loss function designed to prioritize learning depth maps at closer distances rather than farther ones due to the higher significance of nearer depth estimates for odometry accuracy.
- We evaluate our methods with existing approaches in zero-shot indoor scenes. It is important to note that, unlike existing monocular odometry methods, we do not require a scale for evaluation.

On acceptance, we will open-source the coded simulator, CodedVO dataset, and our CodedVO framework for robotics applications at <http://prg.cs.umd.edu/CodedVO>.

#### B. Organization of the paper

The paper is structured in the following sections. Sec. II discusses the existing depth and odometry estimation methods. Sec. III explains the CodedVO framework along with the camera system setup, data generation, and our CodedVO model. Sec. IV illustrates the experimental setup and demonstrates the advantage of coded apertures in overcoming the scale ambiguity in robot navigation. We compare and contrast our results both qualitatively and quantitatively with the state-of-the-art methods for both depth and odometry estimation in Secs. IV-B and IV-C respectively. Finally, we conclude our findings and remark on the potential for future work in Sec. V.

## II. RELATED WORKS

### A. Monocular Depth Estimation

Bhat et. al [8] introduced to learn generalized depth estimation with metric scale in unknown scenes, utilizing MiDaS [9] for depth estimation and performing a lightweight metric binning method to recover the scale. Although these depth models result in state-of-art scale factors on the pre-trained 12 datasets, they still lack in generalization to other novel datasets – both the real world and simulated. To have more generalizability in monocular metric depth estimation in zero-shot samples, Yin et. al [10] demonstrated that the camera model plays an important role. By proposing a canonical camera space transformation module that explicitly addresses the ambiguity problem, they achieved state-of-the-art performance on zero-shot data. Fundamentally, they rely on the defocus model of the sensor system for depth prediction.

### B. Depth from Defocus

In the field of computational imaging, researchers have utilized the camera model to their advantage to estimate metric depth from single images by modifying the camera apertures. The addition of passive elements on the aperture plane has been commonly studied with applications in light-field imaging [11] and depth estimation [12], [13]. It is well known that the depth-dependent defocus ‘bokeh’ or point spread function (PSF) depends on the amplitude and phase of the aperture used. Thus, the two most commonly used coded apertures are (a) Amplitude mask [12] and (b) Phase mask [14]. PhaseCam3D [14] and related works [15], [16] have demonstrated the superior nature of phase masks over amplitude masks due to two main advantages (a) Unlike amplitude masks, phase masks do not block incoming light and hence deliver a higher signal-to-noise ratio and (b) higher depth resolution by designing PSFs to have more variability over depth [14].

### C. Visual Odometry

Geometry-based methods encompass a range of techniques across various sensor modalities. In monocular VO, feature-based methods have consistently demonstrated robust and real-time performance [17]. Direct methods [18] utilizes a probabilistic model, minimizing the photometric error for odometry estimates. Hybrid methods such as SVO [19], demonstrate a semi-direct visual odometry algorithm and achieve real-time performance by eliminating the need for high-cost feature extraction and robust matching. LSD-SLAM [20] proposes a direct featureless method for large-scale environments by utilizing pose-graph optimization. In Stereo-based systems, StereoScan [21] and Stereo DSO [22] exploit disparities between image pairs to achieve precise motion estimation. Furthermore, [23] and [24] harness depth information to significantly enhance VO accuracy. Recently, [6] demonstrates an improvement in monocular visual odometry by utilizing predicted monocular depth from input images.

## III. CODED VISUAL ODOMETRY

Our CodedVO framework utilizes concepts from computational imaging to estimate depth with metric scale using a monocular camera from a single view. First, we simulate coded or blurred RGB images using all-in-focus (AiF) RGB images and depth maps (Sec. III-A). Then, we train a network to estimate metric depth using only coded RGB images (Sec. III-B). Finally, we combine coded RGB and predicted metric depth sequence as a plug-and-play to existing RGB-D odometry methods (Sec. III-C) to estimate the visual odometry of our CodedVO system.

### A. Coded Optics

Optical cameras capture images based on wavelength and depth-dependent blurs called point-spread-function (PSF) – the response of an optical system to a point source with a specific position and wavelength. A PSF can be simulated using Fourier optics theory [25]. The PSF  $h_d$  induced by the lens system of the camera with specific amplitude modulation  $\mathcal{A}$  and phase modulation  $\phi^M$  is given by:

$$h_d = \left| \mathcal{F} \left( \mathcal{A} \exp \left( i\phi^{DF}(d) + i\phi^M \right) \right) \right|^2 \quad (1)$$

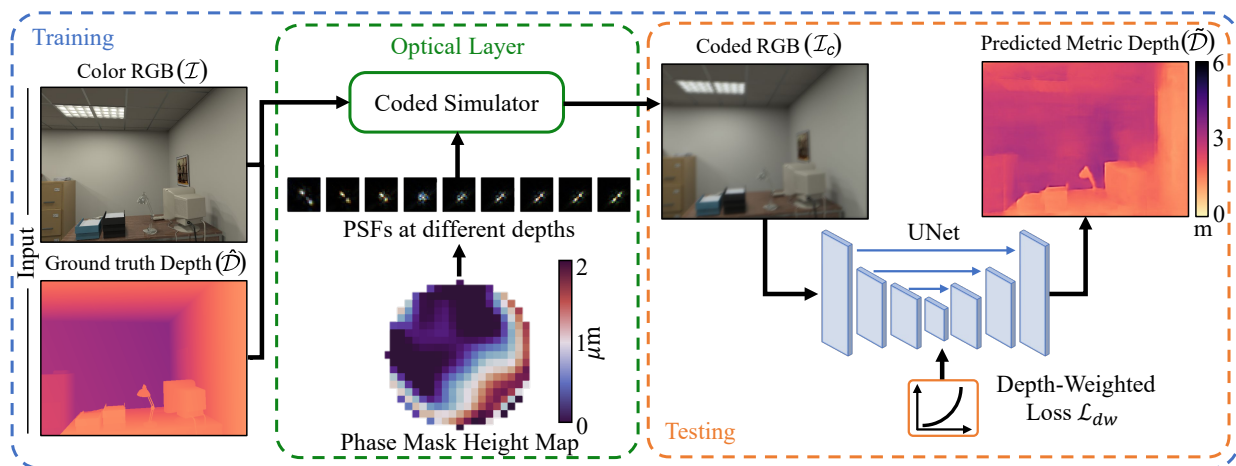


Figure 2: **Metric Depth Prediction Framework:** Our proposed method consists of two parts: (a) a Coded Simulator and (b) a Depth Estimation Network. The coded simulator utilizes RGB-D ground truth input and PSFs to simulate coded blurred RGB images using equation 2. The depth network learns to predict metric depth from image  $\mathcal{I}_c$  captured by a calibrated coded camera.

where  $\phi^{DF}(d)$  is the defocus aberration caused by the point source being  $d$  away from the focal plane and  $\mathcal{F}$  denotes the 2D Fourier transform. Using this model, coded (or blurred) images  $\mathcal{I}_c$  can be generated from AiF images  $\mathcal{I}$  through a nonlinear blurring process from [16]:

$$\mathcal{I}_c = \sum_{d=1}^D \frac{h_d * \mathcal{I}}{h_d * \sum_{d'=1}^d \mathcal{O}_{d'}} \prod_{d'=d+1}^D \left( 1 - \frac{h_d * \mathcal{O}_d}{h_d * \sum_{d'=1}^d \mathcal{O}_{d'}} \right) \quad (2)$$

where  $*$  is the 2D convolution operator and  $\{1, \dots, D\}$  represent a set of discrete depth layers. Here,  $\mathcal{O}_d$ , and  $h_d$  represent the occlusion mask and PSF at depth  $d$  respectively.

Note that  $\mathcal{A}$  must be limited to the range  $[0, 1]$  because optics cannot increase light intensity, but in practice, prior works have constrained  $\mathcal{A}$  as a binary mask for ease in manufacturing. A variety of parameterizations for  $\phi^M$  have been widely explored in the field of computational imaging: Zernike coefficients [15], [26], [27], radially symmetric [16], [28], and pixel-wise [29] – each with a different trade-off in terms of optimizing stability, manufacturing feasibility, and information recovery accuracy (such as depth).

Fig. 2 illustrates the working of our CodedVO depth prediction framework. Our coded simulator inputs AiF  $\mathcal{I}$  and ground truth metric depth map  $\hat{D}$  to output coded RGB frames  $\mathcal{I}_c$  using the aforementioned PSF model. For our work, we utilize a phase mask which is a thin transparent plate with varying thickness that enables us to induce different blur patterns at different distances in the image. The thickness of our phase mask is derived from [14] and ranges from 0 to  $2 \mu\text{m}$  (see Fig. 2). Using the coded simulation that is based on the layered depth of field model [30], we generated a dataset of coded RGB frames and ground truth depth maps. Note that for the predicting depth maps, only  $\mathcal{I}_c$  is used as the input for our depth network.  $\mathcal{I}_c$  can either be simulated from  $\mathcal{I}$  and  $\hat{D}$  or captured directly in the real world through a coded aperture.

### B. Metric Depth Estimation from Defocus

Due to the presence of different blur patterns at different depths, metric depth can be estimated using a single coded image  $\mathcal{I}_c$  [12]. To estimate depth, we adopt a U-Net architecture [31] as it is widely used in pixel-wise prediction tasks. Fig. 2 shows an encoder-decoder architecture with skip connections that take in a 3-channel  $640 \times 480$  coded-image  $\mathcal{I}_c$ . Our convolutional block consists of two  $3 \times 3$  convolutional layers each followed by batch normalization [32] and a rectified linear unit (ReLU). The encoder consists of 5 convolutional blocks, each followed by a  $2 \times 2$  MaxPooling layer. The decoder consists of 5 convolutional blocks and 5 upsampling blocks interleaved. The upsampling blocks include an upsample layer, followed by a single convolutional layer with batch normalization and ReLU.

Traditionally, various methods optimize depth  $\tilde{D}$  or inverse depth maps [14] since the defocus blur is proportional to the inverse of the depth. However, optimizing the model that minimizes depth does not lead to the lowest possible odometry error. This is because existing odometry methods rely on feature correspondence that possesses larger vector lengths for closer distances as compared to correspondences at farther distances in cases of translation motion. Only in cases of pure rotation, the length of correspondences are the same at all depths. Thus, depth accuracy at a closer distance holds a higher value in odometry estimation.

Thus, rather than utilizing the standard  $\mathcal{L}_1$  loss:

$$\mathcal{L}_1 = \frac{1}{N} \sum_{i=1}^N \left| \tilde{D}_i - \hat{D}_i \right| \quad (3)$$

where  $\hat{D}_i$  and  $\tilde{D}_i$  are ground truth depth and predicted depth respectively.  $N$  is the number of pixels per image.

We propose depth-weighted metric loss, enforcing the network to learn depth differently at different depths:

$$\mathcal{L}_{dw} = \frac{1}{N} \sum_{i=1}^N w_{\hat{D}_i} \cdot (\tilde{D}_i - \hat{D}_i)^2; \quad w_{\hat{D}_i} = \alpha^{-\beta \hat{D}_i} \quad (4)$$

$w_{\hat{D}_i}$  is the depth-aware weights of our proposed  $\mathcal{L}_{dw}$  loss that exponentially vary with the ground truth depth. The values of  $\alpha$  and  $\beta$  are chosen empirically as 2 and as 0.3 respectively.

### C. Odometry Estimation

In this work, we plug and play our predicted depth maps in existing RGB-D visual odometry methods such as ORBSLAM [33]. However, for RGB frames, one could either utilize the coded image  $\mathcal{I}_c$  or recover AiF  $\mathcal{I}$  image from  $\mathcal{I}_c$  using different refocusing techniques [11], [34], [35]. However, recovering  $\mathcal{I}$  from  $\mathcal{I}_c$  requires additional computing and is prone to inconsistent errors. Prior computational imaging neural network-based methods [16], [29] generate inconsistent artifacts between frames and hinder the performance of feature correspondences and tracking. Thus, we utilize coded image  $\mathcal{I}_c$  as a tractable alternative RGB input along with our predicted  $\hat{D}$  for RGB-D odometry methods.

Even though  $\mathcal{I}_c$  is *blurry*, it preserves consistency over frames. This is because most odometry methods such as ORB [36] and FAST [37] use pyramidal multi-scale features extraction by subsampling images at different resolutions, reducing the amount of blur at every level. In this paper, we specifically utilize ORBSLAM2 [38] odometry estimation method that relies on ORB features. To ensure a sufficient number of feature detection and matches, we perform a morphological operation – unsharp mask [39] to  $\mathcal{I}_c$  before using it as an input for ORBSLAM2.

## IV. EXPERIMENTS

In this section, we discuss the performance of our CodedVO framework in depth estimation and visual odometry experiments on both standard and custom indoor datasets and evaluate them with state-of-the-art monocular odometry methods with known scales.

### A. Experimental Setup

We test our CodedVO depth estimation framework on a simulated camera setup of  $12 \times 8$  mm sensor size with  $1344 \times 894$  sensor size and  $9.4 \mu\text{m}$  pixel pitch, an approximately 1-inch sensor format that is commonly found in high-end consumer smartphones. We simulate  $\mathcal{I}_c$  using a 50 mm  $f/1.8$  spherical lens and a  $21 \times 21$  phase mask (coded aperture) with  $135 \mu\text{m}$  grid size that ranges 2.835 mm in diameter. We approximate the red, green, and blue channels using discretized wavelengths: 610 nm, 470 nm, and 530 nm, respectively. Our PSFs correspond to the discretized depth layers using a  $23 \times 23$  Zernike parameterized phase mask found in [14]. Furthermore, the depth range  $\mathcal{D}$  is discretized into 27 bins within the interval of  $[0.5, 6]$  meters with a focal distance of 85 cm, making our system suitable for indoor navigation tasks. It is also important to note that we only utilize simulated coded images. Still, methods such as [14], [16] demonstrate how the sim-to-real gap can be minimized to fine-tune the prediction model in real-world coded cameras. In the real world, these coded apertures can be designed and fabricated using photolithography. A two-photon lithography 3D printer (Photonic Professional GT) is commonly used to print such apertures. Once printed, these apertures are typically placed at the focal plane between the camera sensor and the lens.

To train our depth prediction U-Net model, we simulate coded images  $\mathcal{I}_c$  from AiF images  $\mathcal{I}$  and ground truth depth maps  $\hat{D}$  in two different datasets for better generalizability – NYUv2 [40] and our Blender® Eevee rendering engine based UMD-CodedVO dataset. Our UMD-CodedVO dataset contains three indoor sequences – LivingRoom, DiningRoom and Corridor out of which only LivingRoom sequence is used for training purposes. In our experiment, we trained on 1000 samples from each of the two datasets. We set the learning rate at  $10^{-4}$  and a batch size of 3 for training. Both the training and testing procedures were performed on an NVIDIA® GeForce RTX™ 4090. All of our implementations were carried out in PyTorch.

### B. Metric Depth Estimation

To show the robustness of our metric depth estimation model, we evaluate it on five zero-shot indoor datasets – iBIMS-1 [41], two scenes from ICL-NUIM [42], and UMD-CodedVO dataset (Corridor and DiningRoom). Without any fine-tuning or scale adjustment, we compare our depth estimation performance with state-of-the-art (SOTA) methods that are trained on diverse datasets and for hundreds of epochs. Since we require both  $\mathcal{I}$  and  $\hat{D}$  for the generation of coded images  $\mathcal{I}_c$ , we rely on simulated datasets for evaluation. We evaluate our model with three different variations – (a) AiF input  $\mathcal{I}$  with  $\mathcal{L}_{dw}$  loss, (b) Coded input  $\mathcal{I}_c$  with  $\mathcal{L}_1$  loss and (c)  $\mathcal{I}_c$  input with  $\mathcal{L}_{dw}$  loss. We benchmark our predicted metric depth  $\hat{D}$  up to 6m depth range with existing zero-shot metric depth estimation models ZoeDepth [8] and Metric3D [10], utilizing their respective best models for depth prediction. It is important to note that for depth prediction, both ZoeDepth [8] and Metric3D [10] use  $\mathcal{I}$  as input frames, while our approach relies only on  $\mathcal{I}_c$ . We evaluate the depth predictions on three error metrics – (a) Absolute relative error (Abs-Rel), (b) Percentage of depth error under threshold ( $\delta_1 < 1.25$ ), and (c) Root mean squared error (RMS).

Fig. 3 shows a qualitative benchmark of our method with existing methods. Note that [8] and [10] have better normalized depth (and visualization) than our approach, they suffer from incorrect depth scale recovery. Additionally, upon a detailed examination of our methods, it is evident that the depth performance at closer distances is superior in  $\mathcal{L}_{dw}$  as compared to  $\mathcal{L}_1$ . Table I illustrates the performance metrics. Our CodedVO depth network consistently demonstrates strong performance across all datasets. To ensure a fair comparison, we employed ZoeDepth’s best generalizable model (ZoeD-M12-NK) that showed comparable performance only in the ICL-NUIM ( $\circ\text{f}$ ) dataset. Metric3D, a method that emphasizes image transformation into canonical space through focal length adjustment for enhanced metric accuracy, did not yield promising results on our zero-shot test samples. For CodedVO AiF Depth evaluation, we train our depth estimation network with  $\mathcal{I}$  as input rather than  $\mathcal{I}_c$ . It is important to note that our model was trained on a relatively small dataset of only 2000 images, while ZoeDepth benefits from a significantly larger training dataset, potentially affecting its real-time performance. Our model achieves a high inference speed of 858 fps on a 4090 GPU as compared to Metric3D (260 fps) and ZoeDepth (10.67 fps).

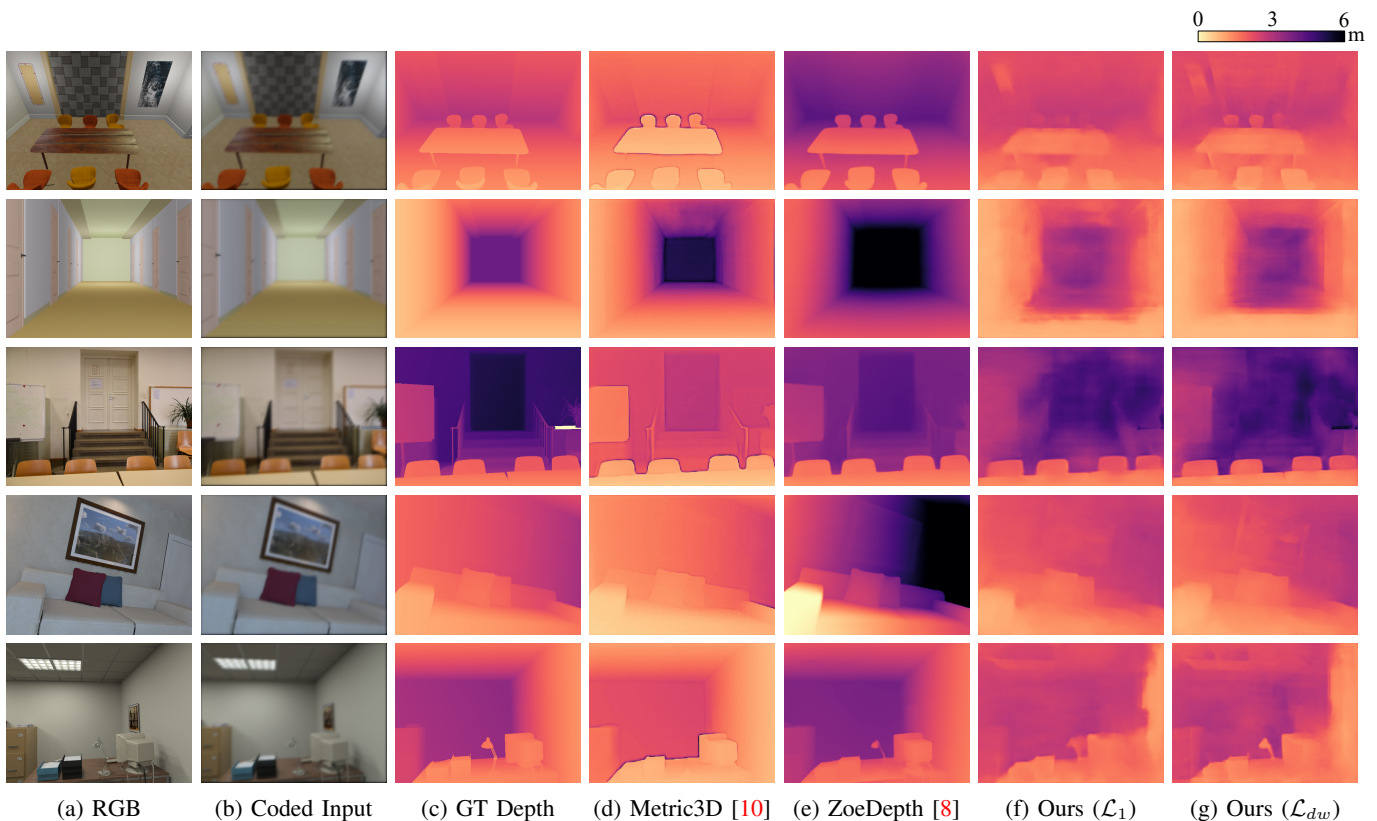


Figure 3: **Qualitative Evaluation: Depth Prediction.** Depth comparison for different datasets (top to bottom): UMD-CodedVO (DiningRoom and Corridor), iBIM-1 [41], ICL-NUIM (lr) [42] and ICL-NUIM (of) [42] with existing metric depth estimation methods.

Method	ICL-NUIM(lr-krt2)			ICL-NUIM(of-krt2)			UMD-CodedVO Dining			iBIMS-1		
	$\delta_1$ ( $\uparrow$ )	Abs-Rel ( $\downarrow$ )	RMSE ( $\downarrow$ )	$\delta_1$ ( $\uparrow$ )	Abs-Rel ( $\downarrow$ )	RMSE ( $\downarrow$ )	$\delta_1$ ( $\uparrow$ )	Abs-Rel ( $\downarrow$ )	RMSE ( $\downarrow$ )	$\delta_1$ ( $\uparrow$ )	Abs-Rel ( $\downarrow$ )	RMSE ( $\downarrow$ )
ZoeD-M12-NK	0.69	0.256	0.549	0.87	0.15	0.434	0.106	0.369	0.831	0.615	0.186	0.777
Metric-3D (CSTM_label)	0.05	0.81	2.27	0.00	0.84	2.49	0.001	0.767	1.676	0.907	0.16	0.521
CodedDepth AiF (Ours)	0.434	0.368	0.880	0.529	0.232	0.820	0.481	0.269	0.662	0.299	0.383	1.422
CodedDepth- $\mathcal{L}_1$ (Ours)	0.913	0.117	0.347	0.821	0.125	0.512	0.987	0.062	0.176	<b>0.911</b>	0.099	0.421
CodedDepth- $\mathcal{L}_{dw}$ (Ours)	<b>0.941</b>	<b>0.088</b>	<b>0.263</b>	<b>0.89</b>	<b>0.097</b>	<b>0.412</b>	<b>0.995</b>	<b>0.052</b>	<b>0.150</b>	0.94	<b>0.08</b>	<b>0.348</b>

Table I: **Quantative comparison with SOTA Metric Depth estimation methods on unseen sequences and benchmarking iBIMS-1 [41] dataset** We evaluate different losses for our method for our approach, comparing them with ZoeDepth [8] and Metric3D [10] models across key metrics:  $\delta_1$ , Abs-Rel, RMSE (meters). The best results are in bold.

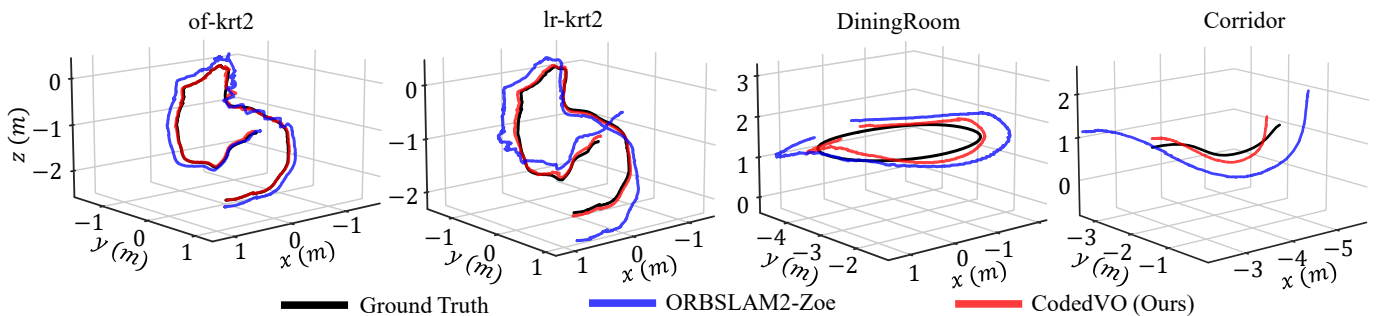


Figure 4: **Trajectory comparison on ICL-NUIM [42] (of-krt2 and lr-krt2) and UMD-CodedVO (Dining and Corridor).** We compare the performance of ORBSLAM2 that utilizes ZoeDepth and our Coded Depth ( $\mathcal{L}_{dw}$ ) as the depth input for ORB-SLAM2.

To illustrate the significance of the depth-weighted loss function  $\mathcal{L}_{dw}$  over standard  $\mathcal{L}_1$ , we compare overall absolute

error  $l_1$  and  $l_1$  error under 3m. Table II indicates that our model trained with  $\mathcal{L}_{dw}$  loss consistently achieves superior

depth estimation performance with  $l_1$  metric under 3m for the ICL-NUIM dataset. We deliberately chose 3m as our threshold as it aligns with ORBSLAM2’s [38] default depth threshold parameter for visual odometry.

Unlike Metric3D and ZoeDepth, CodedVO does not require a large complex neural network architecture due to additive optical constraints for metric depth estimation. Despite producing lower resolution and visually less smooth outputs, our method achieves substantially higher metric depth accuracy compared to previous methods. Our model is parsimoniously designed for visual odometry applications, demonstrating superior numerical, especially in pixels under the 3m range.

Method	lr-krf1		of-krf1	
	$l_1(\downarrow)$	$l_1 < 3m(\downarrow)$	$l_1(\downarrow)$	$l_1 < 3m(\downarrow)$
ZoeD-M12-NK	0.306	0.289	0.500	0.503
CodedDepth AiF (Ours)	0.475	0.404	0.564	0.458
CodedDepth ( $\mathcal{L}_1$ ) (Ours)	<b>0.133</b>	0.177	0.319	0.210
CodedDepth ( $\mathcal{L}_{dw}$ ) (Ours)	0.160	<b>0.128</b>	<b>0.255</b>	<b>0.185</b>

Table II: Metric depth comparison on pixels at all-depth vs pixels under 3m on ICL-NUIM [42] dataset.

### C. Visual Odometry Evaluation

Integrating predicted metric depth from our CodedVO model that utilizes coded aperture into existing RGB-D VO frameworks shows substantial odometry improvements. We evaluate our odometry results on the standard indoor odometry ICL-NUIM [42] dataset and our UMD-CodedVO dataset, featuring challenging scenes such as DiningRoom and a Corridor with low texture surfaces. To ensure an unbiased evaluation, these testing sequences were not a part of the training regime. As our baseline odometry framework, we opted for ORB-SLAM2 with disabled loop closure. The Absolute Trajectory Error (ATE) is the metric used to assess odometry accuracy. We compare and contrast our method with existing methods (see Table III) that either use (a) traditional RGB sensors or (b) RGB-D sensors (like Intel D435i). For evaluating methods that utilize only the traditional RGB sensors, the ATE is estimated after the scale recovery, except for ORBSLAM2-Zoe. ORBSLAM2-Zoe estimates odometry using an RGB-D variant of ORBSLAM2 [38] that uses RGB and metric depth from ZoeDepth [8] as the input. Methods that utilize only RGB images as an input, such as DPVO [43], SVO, and DSO, tend to exhibit higher ATE than approaches leveraging RGB-D input. The results for DPVO, SVO and DSO are obtained from [44] and [43]. Moreover, due to a lack of metric constraints, these RGB-based methods can only result in odometry estimates with an unknown scale whereas methods involving RGB-D input require an additional depth sensor. In Table III, methods from (b) and (c) estimate visual odometry trajectories along with the known metric scale, making them suitable for real-world robotics applications. Fig. 4 illustrates a comparison of visual odometry trajectories obtained from a monocular RGB sensor. Quantitatively, for the UMD-CodedVO Dining dataset, ATE (in meters) for CodedVO ( $\mathcal{L}_{dw}$ ) and ORBSLAM2-Zoe are 0.232 and 0.663, respectively. For UMD-CodedVO Corridor, it is 0.157 and 0.861, respectively. Note that we only qualitatively evaluate

Method	lr-kt0	lr-kt1	lr-kt2	of-kt1	of-kt2	Avg.
(a) RGB Sensor						
DPVO [43]	0.07	0.07	0.02	0.012	0.02	0.03
SVO [44]	0.02	0.07	0.10	0.28	0.14	0.12
DSO [45]	0.01	0.02	0.06	0.83	0.36	0.26
ORBSLAM2-Zoe [8]	0.176	0.055	0.36	0.308	0.13	0.20
(b) RGB-D Sensor						
ORB-SLAM2 [46]	0.01	0.18	0.02	0.04	0.02	0.05
DROID-SLAM [47]	0.25	0.03	0.17	0.08	0.18	0.14
(c) Coded RGB Sensor						
AiF (Ours)	0.511	0.1	0.93	0.11	0.59	0.450
CodedVO ( $\mathcal{L}_1$ ) (Ours)	<b>0.05</b>	<b>0.12</b>	0.10	<b>0.10</b>	0.07	0.084
CodedVO ( $\mathcal{L}_{dw}$ ) (Ours)	<b>0.05</b>	<b>0.12</b>	<b>0.07</b>	<b>0.10</b>	<b>0.05</b>	<b>0.080</b>

Table III: Trajectory evaluation on ICL-NUIM [42] benchmark. Note that methods in teal color utilize only a monocular camera and result in odometry output with scale. Computing ATE for DPVO, SVO and DSO methods requires scale for alignment. Other methods do not require any scale alignment or correction for ATE computations. For each sequence, the median is reported across five independent trials. Here, bold numbers represent the lowest ATE in a given dataset.

with ORBSLAM2-Zoe since it is the best-performing method that results in camera trajectory with a known scale.

Our method utilizes predicted depth  $\tilde{D}$  from coded images  $\mathcal{I}_c$  and is seamlessly incorporated into existing RGB-D visual odometry or Simultaneous Localization and Mapping (SLAM) frameworks, allowing for a comprehensive comparison without requiring any scale alignment. It is important to note that our method consistently outperforms RGB inputs across all methods and achieves comparable performance to an RGB-D dual sensor input data. For a fair comparison, ORB-SLAM2 and DROID-SLAM results are reported without loop closure. It is important to note that  $\mathcal{L}_{dw}$  model consistently performs equally or better than our  $\mathcal{L}_1$  model on ICL-NUIM data (see Table III), especially in scenes with a large number of pixels closer to the camera. By employing the  $\mathcal{L}_{dw}$  loss with optical constraints from a phase mask coded optics, we achieve state-of-the-art monocular visual odometry with a known scale – saving the size, area, weight and power budget of a typical robot system. We successfully achieved an average of 0.08m ATE on the standard odometry ICL-NUIM dataset.

## V. CONCLUSION

In this paper, we introduced CodedVO, a novel monocular visual odometry method that results in state-of-the-art visual odometry, addressing the critical challenge of scale ambiguity in monocular vision. Our method integrates coded RGB input with predicted depth maps in novel scenes and achieves an ATE of 0.08m trajectory error in the standard ICL-NUIM indoor dataset. We demonstrate the effectiveness of optical constraints in a 1-inch monocular RGB sensor with a coded aperture for visual odometry. We believe that this research will serve as a foundational step in leveraging optical and defocus constraints, thereby unlocking new potential for tiny and resource-constrained robots.

## REFERENCES

- [1] N. G. Cervino, A. J. Elias-Costa, M. O. Pereyra, and J. Faivovich, “A closer look at pupil diversity and evolution in frogs and toads,” *Proceedings of the Royal Society B*, vol. 288, no. 1957, p. 20211402, 2021.

- [2] L. M. Mähger, R. T. Hanlon, J. Håkansson, and D.-E. Nilsson, “The w-shaped pupil in cuttlefish (*sepia officinalis*): functions for improving horizontal vision,” *Vision Research*, vol. 83, pp. 19–24, 2013.
- [3] H. Arnoldt, S. H. Strogatz, and M. Timme, “Toward the darwinian transition: switching between distributed and speciated states in a simple model of early life,” *Physical Review E*, vol. 92, no. 5, p. 052909, 2015.
- [4] T. Zhang, X. Hu, J. Xiao, and G. Zhang, “A survey of visual navigation: From geometry to embodied ai,” *Engineering Applications of Artificial Intelligence*, vol. 114, p. 105036, 2022.
- [5] M. O. Aqel, M. H. Marhaban, M. I. Saripan, and N. B. Ismail, “Review of visual odometry: types, approaches, challenges, and applications,” *SpringerPlus*, vol. 5, pp. 1–26, 2016.
- [6] L. Sun, W. Yin, E. Xie, Z. Li, C. Sun, and C. Shen, “Improving monocular visual odometry using learned depth,” *IEEE Transactions on Robotics*, vol. 38, no. 5, pp. 3173–3186, 2022.
- [7] Y. Shechtman, L. E. Weiss, A. S. Backer, S. J. Sahl, and W. Moerner, “Precise three-dimensional scan-free multiple-particle tracking over large axial ranges with tetrapod point spread functions,” *Nano letters*, vol. 15, no. 6, pp. 4194–4199, 2015.
- [8] S. F. Bhat, R. Birkl, D. Wofk, P. Wonka, and M. Müller, “Zoedepth: Zero-shot transfer by combining relative and metric depth,” *arXiv preprint arXiv:2302.12288*, 2023.
- [9] R. Birkl, D. Wofk, and M. Müller, “Midas v3. 1—a model zoo for robust monocular relative depth estimation,” *arXiv preprint arXiv:2307.14460*, 2023.
- [10] W. Yin, C. Zhang, H. Chen, Z. Cai, G. Yu, K. Wang, X. Chen, and C. Shen, “Metric3d: Towards zero-shot metric 3d prediction from a single image,” in *Proceedings of the IEEE/CVF International Conference on Computer Vision*, pp. 9043–9053, 2023.
- [11] A. Veeraraghavan, R. Raskar, A. Agrawal, A. Mohan, and J. Tumblin, “Dappled photography: Mask enhanced cameras for heterodyned light fields and coded aperture refocusing,” *ACM Trans. Graph.*, vol. 26, no. 3, p. 69, 2007.
- [12] A. Levin, R. Fergus, F. Durand, and W. T. Freeman, “Image and depth from a conventional camera with a coded aperture,” *ACM transactions on graphics (TOG)*, vol. 26, no. 3, pp. 70–es, 2007.
- [13] Y. Takeda, S. Hiura, and K. Sato, “Fusing depth from defocus and stereo with coded apertures,” in *Proceedings of the IEEE Conference on Computer Vision and Pattern Recognition*, pp. 209–216, 2013.
- [14] Y. Wu, V. Boominathan, H. Chen, A. Sankaranarayanan, and A. Veeraraghavan, “Phasecam3d—learning phase masks for passive single view depth estimation,” in *2019 IEEE International Conference on Computational Photography (ICCP)*, pp. 1–12, IEEE, 2019.
- [15] J. Chang and G. Wetzstein, “Deep optics for monocular depth estimation and 3d object detection,” in *Proc. IEEE ICCV*, 2019.
- [16] H. Ikoma, C. M. Nguyen, C. A. Metzler, Y. Peng, and G. Wetzstein, “Depth from defocus with learned optics for imaging and occlusion-aware depth estimation,” *IEEE International Conference on Computational Photography (ICCP)*, 2021.
- [17] M. He, C. Zhu, Q. Huang, B. Ren, and J. Liu, “A review of monocular visual odometry,” *The Visual Computer*, vol. 36, no. 5, pp. 1053–1065, 2020.
- [18] J. Engel, V. Koltun, and D. Cremers, “Direct sparse odometry,” *IEEE transactions on pattern analysis and machine intelligence*, vol. 40, no. 3, pp. 611–625, 2017.
- [19] C. Forster, M. Pizzoli, and D. Scaramuzza, “Svo: Fast semi-direct monocular visual odometry,” in *2014 IEEE international conference on robotics and automation (ICRA)*, pp. 15–22, IEEE, 2014.
- [20] J. Engel, T. Schöps, and D. Cremers, “Lsd-slam: Large-scale direct monocular slam,” in *European conference on computer vision*, pp. 834–849, Springer, 2014.
- [21] A. Geiger, J. Ziegler, and C. Stiller, “Stereoscan: Dense 3d reconstruction in real-time,” in *2011 IEEE intelligent vehicles symposium (IV)*, pp. 963–968, Ieee, 2011.
- [22] R. Wang, M. Schworer, and D. Cremers, “Stereo dso: Large-scale direct sparse visual odometry with stereo cameras,” in *Proceedings of the IEEE International Conference on Computer Vision*, pp. 3903–3911, 2017.
- [23] C. Kerl, J. Sturm, and D. Cremers, “Dense visual slam for rgb-d cameras,” in *2013 IEEE/RSJ International Conference on Intelligent Robots and Systems*, pp. 2100–2106, IEEE, 2013.
- [24] G. Hu, S. Huang, L. Zhao, A. Alempijevic, and G. Dissanayake, “A robust rgb-d slam algorithm,” in *2012 IEEE/RSJ International Conference on Intelligent Robots and Systems*, pp. 1714–1719, IEEE, 2012.
- [25] J. W. Goodman, *Introduction to fourier optics*. Freeman, 2017.
- [26] Y. Shechtman, S. J. Sahl, A. S. Backer, and W. E. Moerner, “Optimal point spread function design for 3d imaging,” *Phys. Rev. Lett.*, vol. 113, p. 133902, Sep 2014.
- [27] Y. Wu, V. Boominathan, H. Chen, A. Sankaranarayanan, and A. Veeraraghavan, “Phasecam3d—learning phase masks for passive single view depth estimation,” in *2019 IEEE International Conference on Computational Photography (ICCP)*, pp. 1–12, IEEE, 2019.
- [28] X. Dun, H. Ikoma, G. Wetzstein, Z. Wang, X. Cheng, and Y. Peng, “Learned rotationally symmetric diffractive achromat for full-spectrum computational imaging,” *Optica*, vol. 7, pp. 913–922, Aug 2020.
- [29] X. Liu, L. Li, X. Liu, X. Hao, and Y. Peng, “Investigating deep optics model representation in affecting resolved all-in-focus image quality and depth estimation fidelity,” *Opt. Express*, vol. 30, pp. 36973–36984, Sep 2022.
- [30] C. Scofield, “212-d depth-of-field simulation for computer animation,” in *Graphics Gems III (IBM Version)*, pp. 36–38, Elsevier, 1992.
- [31] O. Ronneberger, P. Fischer, and T. Brox, “U-net: Convolutional networks for biomedical image segmentation,” in *Medical Image Computing and Computer-Assisted Intervention—MICCAI 2015: 18th International Conference, Munich, Germany, October 5–9, 2015, Proceedings, Part III 18*, pp. 234–241, Springer, 2015.
- [32] S. Ioffe and C. Szegedy, “Batch normalization: Accelerating deep network training by reducing internal covariate shift,” in *International conference on machine learning*, pp. 448–456, pmlr, 2015.
- [33] R. Mur-Artal, J. M. M. Montiel, and J. D. Tardos, “Orb-slam: a versatile and accurate monocular slam system,” *IEEE transactions on robotics*, vol. 31, no. 5, pp. 1147–1163, 2015.
- [34] S. Elmalem, R. Giryes, and E. Marom, “Learned phase coded aperture for the benefit of depth of field extension,” *Optics express*, vol. 26, no. 12, pp. 15316–15331, 2018.
- [35] H. Saito and K. Saito, “Image focusing analysis using coded aperture made of a printed mask,” *Japanese Journal of Applied Physics*, vol. 58, no. SK, p. SKKA01, 2019.
- [36] E. Rublee, V. Rabaud, K. Konolige, and G. Bradski, “Orb: An efficient alternative to sift or surf,” in *2011 International conference on computer vision*, pp. 2564–2571, Ieee, 2011.
- [37] E. Rosten, R. Porter, and T. Drummond, “Faster and better: A machine learning approach to corner detection,” *IEEE transactions on pattern analysis and machine intelligence*, vol. 32, no. 1, pp. 105–119, 2008.
- [38] R. Mur-Artal and J. D. Tardós, “ORB-SLAM2: an open-source SLAM system for monocular, stereo and RGB-D cameras,” *IEEE Transactions on Robotics*, vol. 33, no. 5, pp. 1255–1262, 2017.
- [39] D. F. Malin, “Unsharp masking,” *AAS Photo Bulletin*, vol. 16, pp. 10–13, 1977.
- [40] P. K. Nathan Silberman, Derek Hoiem and R. Fergus, “Indoor segmentation and support inference from rgb-d images,” in *ECCV*, 2012.
- [41] T. Koch, L. Liebel, F. Fraundorfer, and M. Körner, “Evaluation of cnn-based single-image depth estimation methods,” in *Proceedings of the European Conference on Computer Vision Workshops (ECCV-W5) (L. Leal-Taixé and S. Roth, eds.)*, pp. 331–348, Springer International Publishing, 2019.
- [42] A. Handa, T. Whelan, J. McDonald, and A. Davison, “A benchmark for RGB-D visual odometry, 3D reconstruction and SLAM,” in *IEEE Intl. Conf. on Robotics and Automation, ICRA*, (Hong Kong, China), May 2014.
- [43] Z. Teed, L. Lipson, and J. Deng, “Deep patch visual odometry,” *arXiv preprint arXiv:2208.04726*, 2022.
- [44] C. Forster, Z. Zhang, M. Gassner, M. Werlberger, and D. Scaramuzza, “Svo: Semidirect visual odometry for monocular and multicamera systems,” *IEEE Transactions on Robotics*, vol. 33, no. 2, pp. 249–265, 2017.
- [45] J. Engel, V. Koltun, and D. Cremers, “Direct sparse odometry,” *IEEE Transactions on Pattern Analysis and Machine Intelligence*, mar 2018.
- [46] R. Mur-Artal and J. D. Tardós, “Orb-slam2: An open-source slam system for monocular, stereo, and rgb-d cameras,” *IEEE Transactions on Robotics*, vol. 33, no. 5, pp. 1255–1262, 2017.
- [47] Z. Teed and J. Deng, “Droid-slam: Deep visual slam for monocular, stereo, and rgb-d cameras,” in *Advances in Neural Information Processing Systems (M. Ranzato, A. Beygelzimer, Y. Dauphin, P. Liang, and J. W. Vaughan, eds.)*, vol. 34, pp. 16558–16569, Curran Associates, Inc., 2021.